Enhanced magnetic separation and photocatalytic activity of nitrogen doped titania photocatalyst supported on strontium ferrite

Azrina Abd Aziz, Kok Soon Yong, Shaliza Ibrahim, Saravanan Pichiah*

Department of Civil Engineering, Faculty of Engineering, University of Malaya, 50603 Kuala Lumpur, Malaysia

ARTICLE INFO

ABSTRACT

An enhanced ferromagnetic property, visible light active TiO$_2$ photocatalyst was successfully synthesized by supporting strontium ferrite (SrFe$_{12}$O$_{19}$) onto TiO$_2$ doped with nitrogen (N) and compared with N-doped TiO$_2$. The synthesized catalysts were further characterized with X-ray diffraction (XRD), transmission electron microscope (TEM), energy dispersive X-ray spectroscopy (EDS), BET surface area analysis, vibrating sample magnetometer (VSM), X-ray photon spectroscopy (XPS) and visible light spectroscopy analysis for their respective properties. The XRD and EDS revealed the structural and inorganic composition of N–TiO$_2$ supported on SrFe$_{12}$O$_{19}$. The supported N–TiO$_2$ exhibited a strong ferromagnetic property with tremendous stability against magnetic property losses. It also resulted in reduced band gap (2.8 eV) and better visible light absorption between 400 and 800 nm compared to N-doped TiO$_2$. The photocatalytic activity was investigated with a recalcitrant phenolic compound namely 2,4-dichlorophenol (2,4-DCP) as a model pollutant under direct bright and diffuse sunlight exposure. A complete degradation of 2,4-DCP was achieved with an initial concentration of 50 mg/L for both photocatalysts in 180 min and 270 min respectively under bright sunlight. Similarly the diffuse sunlight study resulted in complete degradation for supported N–TiO$_2$ and >85% degradation N–TiO$_2$, respectively. Finally the supported photocatalyst was separated under permanent magnetic field with a mass recovery ∼98% for further reuse.

© 2011 Elsevier B.V. All rights reserved.

1. Introduction

The advanced oxidation technologies (AOPs), are state-of-art technology for treating wastewater. Among the advanced oxidation processes heterogeneous photocatalysis is one of the prominent systems to degrade various types of organic pollutants in water and wastewater [1–4]. There has been an enormous amount of research and development in this area due to its effectiveness in degrading and mineralising the recalcitrant organic compounds [5]. The extensive occurrence of phenols in wastewater and associated environmental hazards has increased concern over the public health [5,6]. These toxic organic compounds in wastewater effluent are reported to be a massive impediment to the widespread acceptance of water recycling [5,7]. Furthermore, it has major challenge to achieve the effective removal of persistent organic pollutants from wastewater effluent to minimise the risk of pollution problems from such toxic chemicals and make it able to reuse [5]. Conventional methods such as adsorption by activated carbon and ion exchange resins finally generate wastes during the treatment, thus require additional treatment methods and costs as well [5].

Hence, heterogenous photocatalytic oxidation process employing titanium dioxide (TiO$_2$) has emerged as a promising new alternative process for the degradation of these persistent organic pollutants [8,9].

Heterogeneous photocatalysis using TiO$_2$ semiconductors was initially discovered by Fujishima and Honda in 1972 on the photo-induced splitting of water [10]. The process gradually breaks down the contaminant molecule, thus no residue of the original material remains and therefore no sludge requiring disposal to landfill is produced [8,9]. TiO$_2$ is known as the best heterogeneous photocatalyst due to its cost-effective, strong photo oxidative activity, non toxic, chemical stability, resistant against photo and chemical corrosion [11]. Moreover, it exists in three different structural forms, which are anatase, rutile, and brookite. Among them anatase TiO$_2$ has higher photocatalytic reactivity compared to the rest [12]. In general the TiO$_2$ named viz., Degussa P$_{25}$ was highly employed for commercial purposes. In addition it was also studied for the suitability of photocatalytic treatment of wastewater. Such commercialized TiO$_2$ (Degussa P$_{25}$) semiconductor photocatalyst has wide band gap energy (3.20 eV) and hence successfully used as an efficient photocatalyst [13–17]. Unfortunately, it cannot take up the visible light from sunlight due its wide band gap. It can only utilize ultraviolet (UV) radiation ($\lambda < 400$ nm) for photo excitation [17]. However the sunlight contains only 5–6% of UV radiation in

* Corresponding author. Tel.: +60 379677678; fax: +60 379675318.
 E-mail address: pichiahsaravanan@gmail.com (S. Pichiah).

its electromagnetic spectrum. Therefore an external UV source is needed to maximize the photocatalytic activity of such TiO_2 photocatalyst [17]. It becomes a major limitation since it cannot be a sustainable green catalyst for treating the organics in wastewater.

Hence several attempts have been employed to improve the efficiency of TiO_2 photocatalyst in utilizing solar light or precisely daylight as irradiation source. One such modification is made by doping the photocatalyst with transition metal ions, ion implantation, hydrogen plasma reduction of TiO_2, organic dye sensitization, and hydroxide or surface coordination. Doping of the catalyst with metals ion such as Fe, Sb, Co, etc., can extend the absorption spectrum to visible light region (400–800 nm), where the sunlight can be utilized effectively [17,18]. This type of doping was studied comprehensively by few researchers [17,19–21]. Some of their findings are as follows: Sikong et al. [22] in their work prepared Fe-doped TiO_2/SnO_2 by sol–gel method and photoactivity was investigated for *Escherichia coli* killing. The *E. coli* were completely diminished within 90 min under UV radiation and almost 100% inactivated under visible light exposure [22]. Nahar et al. [23] in their study observed that Fe doping increases the UV and visible light performance [23]. Nonmetal ion [24–33] doping such as nitrogen alternatively, narrowed the band gap by the mixture of N 2_p states with O 2_p on the top of valence band at substitutional lattice sites in the form of nitride (Ti–N) or oxynitride (Ti–O–N) [33].

In recent years, magnetic based TiO_2 photocatalyst synthesis has evolved as a mean to resolve the difficulty of separation of TiO_2 photocatalyst from the treated water, by applying an external magnetic field [34]. Till date few reports has been reported of which most findings focused on soft ferromagnetic materials, which is magnetite (Fe_3O_4) that can oxidized to maghemite (γ-Fe_2O_3), which is also ferromagnetic if the particles are heated over 150–170 °C [35–39]. Unfortunately, the nanosized core magnetic materials are easily oxidized and transform rapidly when the heat treatment temperature is over 400 °C [34,40]. Therefore, it is inherently difficult to produce titania-coated particles with high visible light photoactivity without losses of magnetic property.

Hence the major objective of the present work is to develop ferromagnetic property improved TiO_2 photocalyst by supporting it on strontium ferrite ($SrFe_{12}O_{19}$) for enriched recovery and reuse. The objective also focused on visible light absorption by Nitrogen doping onto TiO_2 for utilizing sunlight radiation for excitation. The photocatalytic activity was investigated by degrading a biorecalcitrant and toxic pesticide pollutant viz., 2,4-dichlorophenol (2,4-DCP) under bright and diffused sunlight irradiation.

2. Materials and methods

2.1. Synthesis of N-doped TiO_2

All chemicals were of analytical grade and obtained from Sigma Aldrich, Malaysia. Milli-Q water (>18.2 M Ω cm) was used for all experiments. The N-doped TiO_2 was synthesized by the following technique: an aqueous $Ti_2(SO_4)_3$ was prepared by 20 wt.% of $Ti_2(SO_4)_3$ and 80 wt.% of distilled water. Subsequently, 300 mL of $Ti_2(SO_4)_3$ solution and 1.2 L of Milli-Q water were added into 2 L beaker, then the ready solution was hydrolyzed in magnetic stirring apparatus by the addition of 30% NH_3 aqueous solution until the pH of the mixture reached 7. The hydrolysis product, which is in the form of white suspended semi-solid was rinsed with Milli-Q water until the concentration of the sulphate, SO_4^{2-} in the rinsing water reached 0.5 mg/L. The concentration of SO_4^{2-} was determined using the standard methods for the examination of water and wastewater. Finally, dried and calcined at 500 °C for an hour.

2.2. Synthesis of SiO_2-coated $SrFe_{12}O_{19}$ nanoparticles

$(NaPO_3)_6$ aqueous solution (5%) was prepared using 5 g $(NaPO_3)_6$ and 95 g of Milli-Q water. It was then added into 150 mL $SrFe_{12}O_{19}$ dispersion. As to get the mixed dispersion with 16 wt.% $(NaPO_3)_6$ for $SrFe_{12}O_{19}$, 3.62 g of $SrFe_{12}O_{19}$ was added into Milli-Q water and made up to 150 mL dispersion. It is followed by the addition of 33 mL of $Na_2O·3SiO_2$ solution (10%) into the dispersion to get 200 wt.% $SiO_2/SrFe_{12}O_{19}$ dispersion. The dispersion was sonicated for 15 min in ultrasonic water bath and followed by heating to 90 °C on a magnetic stirrer provided with heater. The pH value of the dispersion was adjusted to ca. 10.0 by titrating H_2SO_4 solution (5%) under vigorous stirring. Further stirring was carried out at 90 °C to obtain a viscous dispersion. A thin SiO_2 layer was deposited on the $SrFe_{12}O_{19}$ nanoparticles. The SiO_2-coated $SrFe_{12}O_{19}$ nanoparticles were washed by centrifugation and redispersed for quite a lot of times with Milli-Q water to prevent them from agglomerating.

2.3. Synthesis of N-doped TiO_2 supported on $SrFe_{12}O_{19}$ photocatalyst

About 6 mL of SiO_2-coated $SrFe_{12}O_{19}$ dispersion (0.15 g) and 1.0 g of N-doped TiO_2 were mixed. Then a small portion of water was added to alter the mixture to be a paste. The mixture was sonicated for 15 min to well mix the substances, then dried, grinded, and calcined for 30 min at 400 °C. Hence, the magnetically separable N-doped TiO_2 supported on $SrFe_{12}O_{19}$ photocatalyst was obtained.

2.4. Characterization of synthesized photocatalyst

The X-ray diffraction (XRD) analysis was performed with Bruker D8 Advance diffractometer using Cu Kα (λ = 1.5406 Å) radiation, to explore the crystal structure and crystallinity of the photocatalyst. The average crystallite size was obtained using the Scherrer's equation ($D = k\lambda/\beta \cos\theta$). A transmission electron microscope (TEM) (Philips CM-12) was performed by dispersing the samples in ethanol and were dispersed using an ultrasonicator (Starsonic, 35) for 15 min and fixed on carbon-coated copper grid to obtain the structure of the prepared photocatalysts at the nanoscale. The inorganic composition of the prepared photocatalysts were analyzed by energy dispersive X-ray spectroscopy (EDS) of Zeiss Auriga® FESEM. Brunauer–Emmett–Teller (BET) surface measurements using nitrogen as adsorption molecule was carried out with Quantachrome 6B Autosorb Automated Gas Sorption System. The degassing of sample was carried out for 5 h at 150 °C. The pore-size distribution curve was obtained from the analysis of the desorption portion of the isotherm using the BJH (Barrett–Joyner–Halenda) method. X-ray photoelectron spectrum (XPS) was obtained from Axis Ultra DLD instrument of KRATOS using monochromatic Al Kα radiation (225 W, 15 mA, 15 kV). The magnetization with applied magnetic field was measured by vibrating sample magnetometer (VSM, Lakeshore 7410) at room temperature. It reveals the magnetic properties like coercivity, saturation magnetization and remanence of the synthesized material. The absorption spectra of the prepared catalysts was analyzed with visible spectrophotometer (Merck, Spectroquant Pharo 100) over a wavelength ranging between 350 and 800 nm. The prepared catalysts were dispersed with distilled water in a quartz cell (10 mm path length), and their spectral was examined. The band gap energy was calculated as per the literature report [41] using the following equation:

$$\text{Band gap energy}\,(E) = \frac{hc}{\lambda} \tag{1}$$

where h is the Planks constant, 6.626×10^{-34} Joules/s, c is the speed of light, 3.0×10^8 m/s, and λ is the cut off wavelength, nm
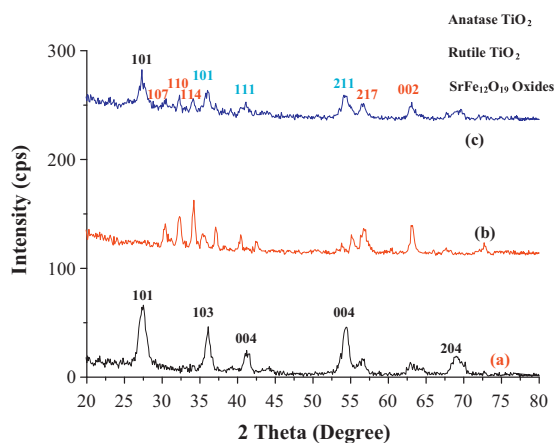
Fig. 1. XRD patterns of (a) N-doped TiO_2 calcined at 500 °C; (b) strontium ferrite coated SiO_2; (c) N–TiO_2 supported on strontium ferrite.

2.5. Photocatalytic activity

The photocatalytic activitiy of the synthesized photocatalyst was evaluated for the degradation of recalcitrant pesticide namely 2, 4-dichlorophenol (2,4-DCP). The evaluations were carried out in a batch reactor of 500 mL capacity, with a working volume of 250 mL under vigorous continuous stirring in presence of both bright and diffused sunlight conditions. The bright sunlight condition refers to complete sunny day with an intensity output varying between 60,000–140,000 lux, similarly the diffused (i.e., not direct sunlight) sunlight condition the intensity varies between 10,000–60,000 lux. The initial 2,4-DCP concentration was fixed at 50 mg/L with a catalyst dosage of 1 g each. Samples were withdrawn at regular interval and analyzed for residual 2,4-DCP concentration using high performance liquid chromatography (HPLC; Perkin Elmer Series 200, UV Detector) after separating the catalyst by centrifugation at $10,000 \times g$. The column employed was C_{18} (Supelco) column (150 mm × 4.6 mm, 5 μm particle size) with acetonitrile/water (60/40) as the mobile phase at a flow rate of 1 ml min^{-1} and the injection volume was 20 μL with UV absorption wavelength being 275 nm. The detection limit of the HPLC was 30 pg mL^{-1}. The evaluation was further runs until complete degradation was ensured. The N–TiO_2 supported $SrFe_{12}O_{19}$ was recovered under a permanent magnetic field and reused for additional runs.

3. Results and discussion

3.1. Structural and morphology characteristics of synthesized photocatalysts

XRD is a vital characterization analysis for the prepared photocatalysts because justifies the change in crystalline phase structure during synthesis and calcinations. The peaks on the XRD patterns of synthesized photocatalysts revealed in Fig. 1 were designated to anatase crystal phase (most active phase) without any indication of other phases, such as rutile (Fig. 1S). It is well known that anatase is more stable than rutile with higher enthalpy of formation [42]. Moreover, this form has been found to exhibit higher photocatalytic processes [34]. This phase transition was achieved due to the moderate calcinations temperature at 500 °C, thus indicates that the synthesized photocatalysts are stable in this heat treatment process. Furthermore, it is proved that the phase transition is caused by the structural strontium and nitrogen doping, i.e. the substitution of this metal and non-metal ions into titanium structural framework
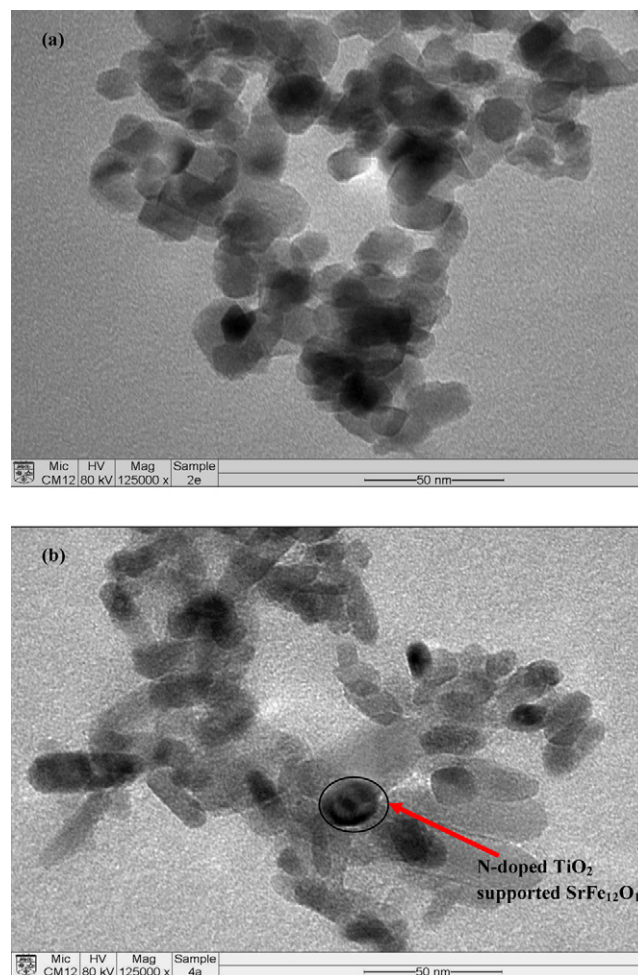
Fig. 2. TEM image of (a) N-doped TiO_2; (b) N–TiO_2 supported on strontium ferrite.

[34]. No significant variations of peaks were found in N-doped TiO_2 (Fig. 1a). The low doping percentage is responsible for the insignificant changes in this crystalline structure. The peaks of the magnetic core SiO_2-coated $SrFe_{12}O_{19}$ can also be observed (Fig. 1b). It is found that there is wide wave peak between 20° and 30°, which shows the characteristics of amorphous SiO_2 [34]. Furthermore, it shows zero extra peaks in N–TiO_2 supported on $SrFe_{12}O_{19}$ (Fig. 1c) signifying that there was no formation of impurities in the synthesized catalyst. The magnetic particles maintain in anatase phase yet have no influence on TiO_2 crystals. However, the intensity decreased due to the coating of N-doped TiO_2 on the magnetic core. In addition the presence of strontium ferrite after supporting N–TiO_2 onto was evident (Fig. 2S). The shell formation of N-doped TiO_2 on the magnetic core might lower the peak intensity. The Joint Committee on Powder Diffraction Standards (JCPDS) peak component fitting to relevant N–TiO_2 phase namely anatase, rutile and strontium ferrite is shown in Figs. 1S and 2S as supplementary data. Similar observation was reported by Xu et al. [34]. In their study, the peaks of $NiFe_2O_4$ were not revealed after doping with N-doped TiO_2 due to the low content of SiO_2 coated $NiFe_2O_4$ nanoparticles disperse uniformly around N-doped TiO_2 congeries. Thus, it suppressed the appearance of $NiFe_2O_4$ XRD peaks.

The calculated crystallite sizes for synthesized photocatalysts are found to be 16.6 nm (N-doped TiO_2) and 28.7 nm (N-doped TiO_2 supported $SrFe_{12}O_{19}$), respectively. It is a general characteristic of the photocatalyst, along with having good physical and chemical stability. The high photocatalytic activity generally depends on the crystallite sizes because the nano size will result in the quantum
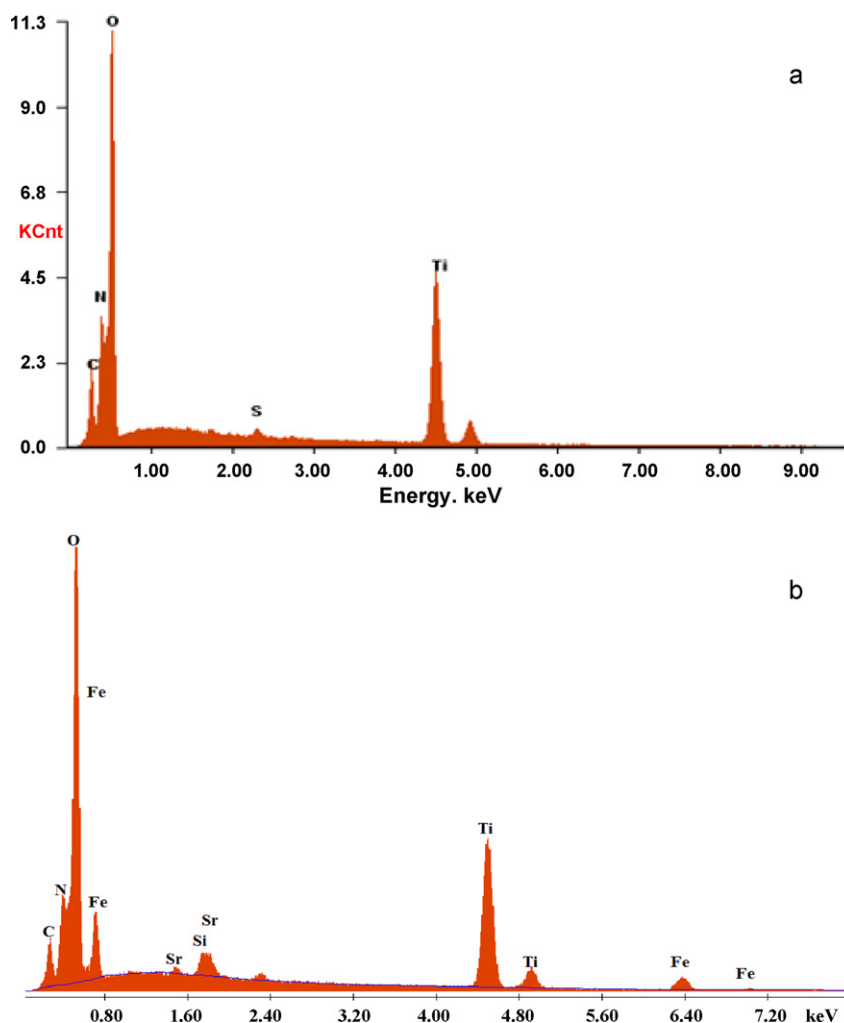
Fig. 3. EDS spectrum image of (a) N-doped TiO$_2$; (b) strontium ferrite supported N–TiO$_2$.

effect, where the electronic properties of solids are changed with the reduction of crystal size. In general if the photocatalyst has particle size less than 100 nm the quantum effect will be dominant and the physical properties will be altered. Nanoparticles of different semiconductors, including anatase and rutile TiO$_2$, have been widely studied during last decade [43–45]. Summarizing, the absorption spectra shift to higher photon energy and develop a discrete character as the size of particles decreases [43–45]. In the present study the prepared photocatalysts had particle size less than 30 nm. This is further confirmed by the TEM pictures (Fig. 2a and b). This reduced particle size will increase the surface to volume ratio, which in turn will contribute to improved thermal, mechanical, and photocatalytic properties of the photocatalyst. The wider peaks of N-doped TiO$_2$ proved that the smaller crystallite sizes caused the XRD peaks broadening [26].

The N-doped TiO$_2$ and N–TiO$_2$ supported SrFe$_{12}$O$_{19}$ were investigated by TEM in order to explore the size and interactions among the components in the synthesized photocatalysts. The obtained micrographs of the prepared N-doped TiO$_2$ and strontium ferrite photocatalysts were depicted in Fig. 2a and b, respectively. The N-doped TiO$_2$ micrograph indicates regular discoidal porous structure and particle shapes of the nanoparticles. However, Fig. 2b shows the agglomeration of irregular porous structure with cylindrical, discoidal, and spherical particle shapes. The micrographs clearly show the supported of SrFe$_{12}$O$_{19}$ onto N-doped TiO$_2$ coagulated in SiO$_2$ coating, thus performed the irregular structure. The occurrences of

the darker contrast are due to the large surface energy of SrFe$_{12}$O$_{19}$ that enter into N–TiO$_2$ shell and proved high electron scattering of SrFe$_{12}$O$_{19}$. The micrographs also showed that the prepared photocatalysts are in the range of nano size (Fig. 3S). Xu et al. [34] in their TEM study reported that the NiFe$_2$O$_4$ nanoparticles are encapsulated in silica coating to form silica–nickel, silica–nickel (SN) after doping [34]. The particle sizes for both synthesized photocatalysts from TEM were less than 30 nm.

The EDS spectra of synthesized photocatalysts are illustrated in Fig. 3a and b. It is specifically observed that the N–TiO$_2$ supported SrFe$_{12}$O$_{19}$ (Fig. 3b) consists of Ti, O, N, Sr, Si, Fe, and C. Each peak is particular to an atom, or resemble to an element. There were distributed due to heating at high temperature. The peak intensity represents the concentration level of the element in the specimen. The photocatalyst having majority of 34.53 wt.% of Ti and 32.73 wt.% of O, respectively. Large amount of Ti indicates correct method of preparation and high photocatalytic efficiency. Meanwhile minority elements include N, Si, Sr, and C, which are less than 10 wt.% and Fe which is the largest portion of dopant, 20.76 wt.%. The significant amount and the high intensity of Fe encourage the photocatalyst for better recovery with strong magnetic property. The results are good certainly because the greater amount of the TiO$_2$, the higher will be the photocatalytic activity, ultimately shows marginally increased surface area of the SrFe$_{12}$O$_{19}$ allow more N-doped TiO$_2$ adhere on the surface of the magnetic core. The credibility of these facts could be then further verified with BET surface area analysis.
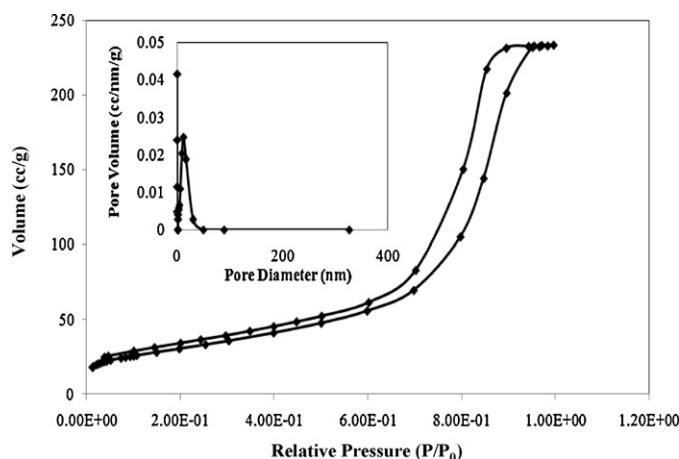
Fig. 4. Adsorption–desorption isotherm and pore size distribution curve and of N-doped TiO₂.

3.2. BET surface area analysis

Figs. 4 and 5 show adsorption–desorption isotherms of the prepared photocatalysts along with the pore size distribution (PSD). The figures indicate that the both synthesized photocatalysts are categorized in type IV, commonly associated with the presence of mesoporosity. The capillary condensation in mesopores gives rise to a hysteresis loop and exhibited a limited uptake at high relative pressure, P/P_0. It contained strong adsorbate (nitrogen gas-adsorbent) interactions. These type of structures resulted from the agglomeration of the primary synthesized photocatalyst particles [34]. In addition, the rounded knee occurred in the isotherms indicates approximate location of monolayer formation and zero micropores filling. The adsorption hysteresis curve pattern showed that the synthesized photocatalyst had cylindrical pore geometry. The average pore sizes are found to be 13.51 and 16.35 nm respectively, which proved that the prepared photocatalysts is a mesopores material. This also indicates that the coating of $SrFe_{12}O_{19}$ into N-doped TiO_2 generously proportioned the pore size of the photocatalyst. The BET specific surface area of N-doped TiO_2 was found to be $106\,m^2/g$ with a total pore volume of $0.3592\,cm^3/g$ compared to $84\,m^2/g$ and $0.3437\,cm^3/g$ for N–TiO_2 supported $SrFe_{12}O_{19}$. The reduced surface area and pore volume is due to strontium ferrite supported on it. The supporting very rarely
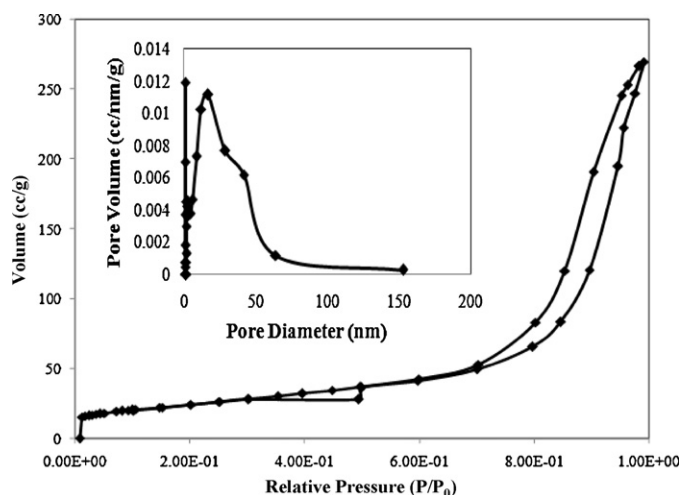
can contribute to the doping in a minor ratio. The accumulation of ferrite particles can also reduce the pore volume by decreasing the pores that can fit into the solid. The smallest crystallite size and higher porosity of N-doped TiO_2, might have resulted in a higher BET surface area. This clarifies that the more N-doped TiO_2 pores can fit in the solid, the smaller these pores will be and resulted in an increasing surface area and higher adsorption capacity. The lowest surface area of N–TiO_2 supported on $SrFe_{12}O_{19}$ nevertheless, gives zero effects on the efficiency of the photocatalytic activity.

3.3. XPS analysis

The chemical state of doped N–TiO_2 was analyzed by XPS consecutively to determine the absorption of nitrogen and strontium into TiO_2 after heat treatment. High resolution XPS spectra of prepared strong ferrite supported TiO_2 photocatalyst are shown in Fig. 6a–c. The spectrum shows the Ti 2_p, Si 2_p, and N1_s shell respectively. The spectra of N–TiO_2 supported on $SrFe_{12}O_{19}$ contains principally Ti, O, N, Fe, and Si elements and a low amount of carbon with a peak at 284.6 eV. The Ti 2_p peaks resulted with a narrow peak at about 458 eV and a broad peak at about 463 eV, which proved that the characteristic for TiO_2 species was revealed. This peak is much higher than that of typical binding energy of TiO_2. These two peaks considered as the active sites for photocatalytic activity especially under visible light irradiation. Similar kind of peaks with different binding energy level was observed by Wang et al. [42] in their study on tin doping in to TiO_2. The present study resulted with an increased binding energy of TiO_2 and thus finally contributing enhanced visible light activity of the photocatalyst [42]. Obvious evidence for the doping of atomic β-N into anatase lattice from XPS spectra is not obtained in the present study. Comparable results are presented in the study from Sano et al. [46]. In their study, the N 1_s XPS spectra of the N-doped TiO_2 suggesting that the N atom near the surface were replaced with O atom during the heat treatment process after Ar⁺ etching. Thus, the β-N atoms did not present in the surface region of the photocatalyst.

3.4. VSM analysis

The ferromagnetic hysteresis obtained from the VSM analysis is depicted in Fig. 7. The figure clearly reveals the ferromagnetic hysteresis behaviour of ferrite supported N–TiO_2. The applied magnetic field was approximately $19.5 \times 10^6\,A\,m^{-1}$ when the magnetization (M_s) moment reached saturation point of 9.6647 emu/g. The intensity of applied magnetic field weakens to zero when the remanence (M_r) magnetism of the photocatalyst is 5.1967 emu/g. The coercivity (H_{ci}) of the photocatalyst of the $SrFe_{12}O_{19}$ is 4187.2 G. This higher magnitude of the coercivity is due to the hard magnet nature of $SrFe_{12}O_{19}$. In general the ferrite material that hold high coercivity value are called as "*hard ferromagnetic*" material and this material embraces good magnetic property which has a very good stability against magnetic property losses. The obtained coercivity proved that the prepared strontium ferrite supported N–TiO_2 is an excellent ferromagnetic material. The obtained hysteresis also supports the same. Thus, the prepared supported photocatalyst can be almost completely recovered with minimum loss, for many numbers of cycles with no diminishing in both the magnetic property and photoactivity.

3.5. UV–vis spectra absorption and band gap energy

The UV–vis absorption spectra of both synthesized photocatalysts were compared and depicted in Fig. 8.. The doping of non-metal ion, nitrogen on TiO_2 indicates that there is a clear extension of absorption range in visible light region and high visible absorbance, 0.12 was observed at 550 nm wavelength. The

Fig. 5. Adsorption–desorption isotherm and pore size distribution curve and of N–TiO₂ supported on strontium ferrite.
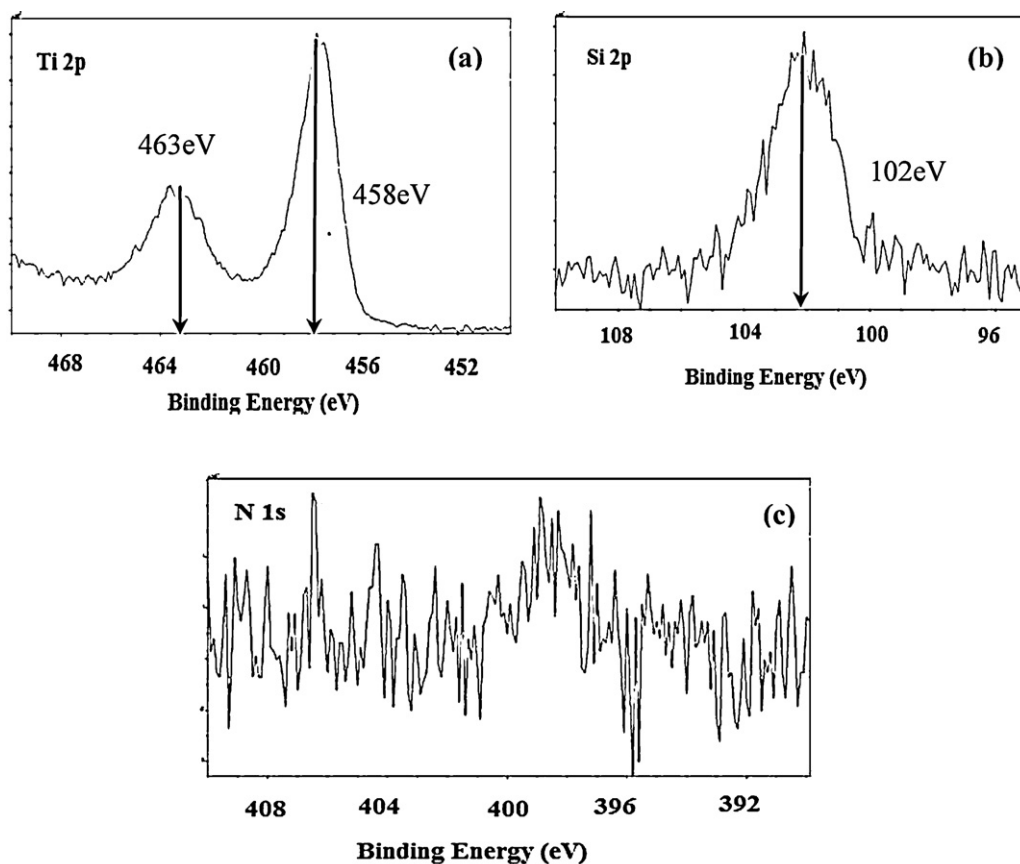
Fig. 6. XPS spectra of strontium ferrite supported N–TiO$_2$ (a) Ti 2$_p$; (b) Si 2$_p$; (c) N 1$_s$.

nitrogen dopant enhances the absorption by providing larger surface area, thus increase capacity of absorption. The N atom isolated with O atom to form impurity energy level and easy to absorb visible light. Besides, it formed oxygen deficient sites that are proved to only emerge visible light and act as blocker for reoxidation. The high consistency in the absorption contributed to the increasing of visible light photocatalytic activity of synthesized photocatalysts. Furthermore, the absorption in the visible light region (0.16) increased upon doping on the silica-coated SrFe$_{12}$O$_{19}$ core. This is an imperative finding as the ferrite magnetic core that dispersed in

TiO$_2$ matrix enhances the absorption in this region. There is clear reduction in the band gap energy for N-doped TiO$_2$ (3.11 eV) and N–TiO$_2$ supported on SrFe$_{12}$O$_{19}$ (2.8 eV). This is lower compared to commercial titania photocatalyst Degussa P$_{25}$, which is 3.2 eV. This revealed that the prepared photocatalysts had lowered the band gap energy between the conduction and valence band, which means the excitation, happened at very lower energy obtained from the visible spectrum of electromagnetic radiation. During N-doping, the 2$_p$ orbital of the dopant N atom interacts with the O 2$_p$ orbital. The interactions creates charge transfer from the dopant to conduction or valence band of titania, thus gives rise to the red shift of absorption [47]. In addition it can contribute much onto improve photoactivity of the prepared catalysts. It also implies that
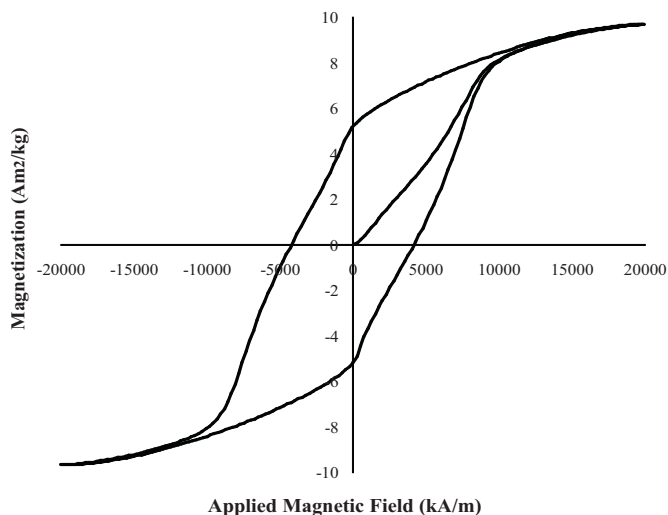
Fig. 7. Ferromagnetic property of strontium ferrite supported N–TiO$_2$.
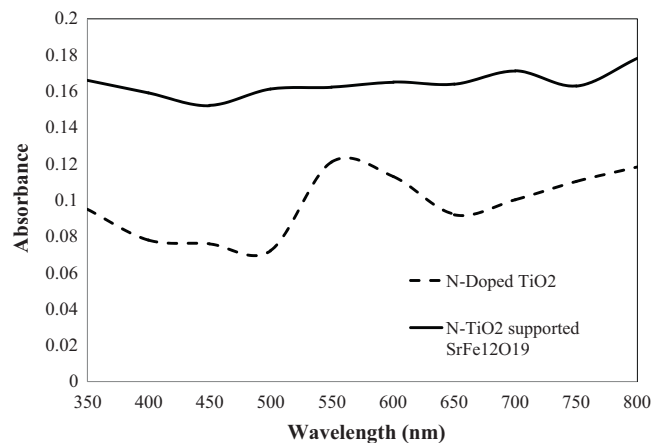
Fig. 8. Visible light absorption spectra of N-doped TiO$_2$ and supported N–TiO$_2$.
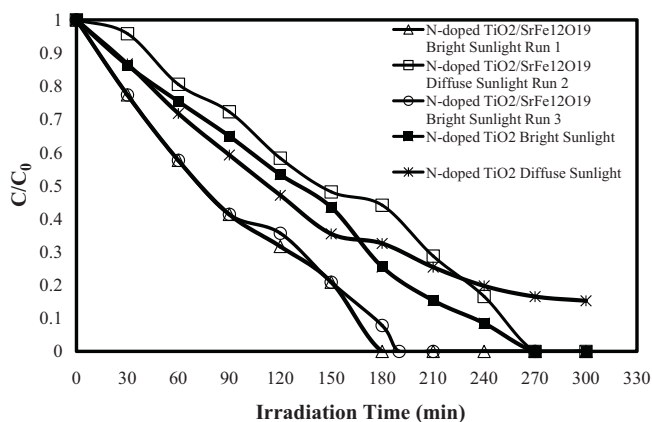
Fig. 9. Photocatalytic activity of N-doped TiO₂ and strontium ferrite supported N–TiO₂ in degrading 2,4 DCP under sunlight illumination.

the synthesized photocatalyst can even excite at lower irradiation of visible light.

3.6. Photocatalytic activity

Fig. 9 illustrates the photocatalytic activity of prepared photocatalysts by degrading of 2,4-dicholorophenol (2,4-DCP) at two different irradiation conditions i.e., under bright and diffused sunlight. The N-doped TiO_2 resulted in 100% degradation of 2,4 DCP in 270 min, while N–TiO_2 supported on $SrFe_{12}O_{19}$ showed similar 100% degradation but in 180 min (Run 1) under bright sunlight. Similarly the results of diffused sunlight experiments also proved the photoactivity of both the photocatalysts, where N–TiO_2 supported $SrFe_{12}O_{19}$ took nearly 270 min with a complete degradation of 2,4-DCP (Run 2). Meanwhile, non-supported catalyst achieved >85% degradation in 300 min. The study revealed that N–TiO_2 supported $SrFe_{12}O_{19}$ photocatalyst showed an excellent photocatalytic activity under both bright and diffused sunlight illumination. The narrowed band gap semiconductor of this photocatalyst ($\sim$2.8 eV) lowered the position of the conduction band, thus the position of valence band is higher than N-doped TiO_2. It was also reported that the SiO_2 layer between titania and iron oxide could weaken the adverse influence of iron oxide, furthermore improve the photocatalytic activity of synthesized photocatalyst even in diffuse sunlight exposure [38]. It was clearly observed there is reduction in BET surface area when N-doped TiO_2 is supported by $SrFe_{12}O_{19}$. However, this reduction surface area seldom hinders the photoactivity of the prepared nanocatalyst (Fig. 9).

Moreover, narrowed band gap energy can effectively reduced the recombination of photogenerated charge carriers and enhance the photocatalytic activity [42]. The photogenerated electrons from conduction band get transferred to trapping sites of anatase phase in presence of sunlight irradiation. Such subsequent transfer of electrons to lattice trapping sites of anatase helps in separating the charge carriers effectively. These trapping sites also benefits by preventing the recombination to a large extent and facilitating the charge separation thereby activating the catalyst. These effects could be observed in both synthesized catalyst, but much largely reflected N–TiO_2 supported $SrFe_{12}O_{19}$. The trial runs were carried out by separating the catalyst under a strong magnetic field. A mass recovery of $\sim$98% was achieved with a minor loss. This loss was expected owing to its nanoparticle size. The recovered runs (Run 2) showed photoactivity similar to that of virgin catalyst (i.e., similar to that of Run 1). The Run 2 took extended time because of the diffused sunlight irradiation. Wang et al. [42], in their study with tin as a dopant onto Titania photocatalyst for visible light enhancement, achieved complete degradation of 4-cholorophenol (4-CP)

in 90 min of irradiation of artificial visible light irradiation with an initial 4-CP concentration of 5×10^{-5} moles/L [42]. However, complete degradation of further recalcitrant pesticide was achieved by natural sunlight along with an additional improved ferromagnetic property for recovery and reuse. Over all the present study revealed the outstanding photoactivity for a sustainable development.

4. Conclusions

The photocatalysis effect of N–TiO_2 supported $SrFe_{12}O_{19}$ on degradation of recalcitrant pesticide namely 2,4-DCP was successfully studied and compared with N-doped TiO_2. The supported photocatalysts exhibited an enhanced structural, morphological and magnetic properties, as well as photocatalytic process under visible light irradiation. The synergistic effect induced by doping of non-metal ion, nitrogen and ferromagnetic materials, $SrFe_{12}O_{19}$ into TiO_2. A higher degradation of 2,4-DCP concentration was achieved under both bright and diffused sunlight for both photocatalysts. The results of the presently prepared photocatalyst supported on strontium ferrite laid a pathway for a green and sustainable catalyst design. This supported catalyst could be a new generation photocatalyst for treating higher toxic wastewater in short duration with improved reuse.

Appendix A. Supplementary data

Supplementary data associated with this article can be found, in the online version, at doi:10.1016/j.jhazmat.2011.10.069.

References

[1] N. Savage, M.S. Diallo, Nanomaterials and water purification. Opportunities and challenges, J. Nanopart. Res. 7 (2005) 331–342.
[2] Y. Liu, J. Li, X. Qiu, C. Burda, Bactericidal activity of nitrogen-doped metal oxide nanocatalysts and the influence of bacterial extracellular polymeric substances (EPS), J. Photochem. Photobiol. A 190 (2007) 94–100.
[3] Q. Yang, H. Choi, D.D. Dionysiou, Nanocrystalline cobalt oxide immobilized on titanium dioxide nanoparticles for the heterogeneous activation of peroxymonosulfate, Appl. Catal. B-Environ. 74 (2007) 170–178.
[4] H. Choi, E. Stathatos, D.D. Dionysiou, Photocatalytic TiO_2 films and membranes for the development of efficient wastewater treatment reuse system, Desalination 202 (2007) 199–206.
[5] S. Ahmed, M.G. Rasul, W.N. Martens, R. Brown, M.A. Hashib, Heterogenous photocatalytic degradation of phenols in wastewater: a review on current status and developments, Desalination 261 (2010) 3–18.
[6] E. Eriksson, A. Baun, P.S. Mikkelsen, A. Ledin, Risk assessment of xenobiotics in stormwater discharged to Harrestup Ao, Denmark, Desalination 215 (2007) 187–197.
[7] N.M. Mahmoodi, M. Armani, N.Y. Lymaee, K. Gharanjig, Photocatalytic degradation of agricultural N-heterucyclic organic pollutants using immobilized nanoparticles of titania, J. Hazard. Mater. 145 (1–2) (2007) 65–71.
[8] I. Oller, W. Gernjak, M.I. Maldonado, L.A. Perez-Estrada, J.A. Sanchez-Perez, S. Malato, Solar photocatalytic degradation of some hazardous water-soluble pesticides at pilot-plant scale, J. Hazard. Mater. 138 Part B (2006) 507–517.
[9] A. Garcýa, A.M. Amat, A. Arques, R. Vicente, M.F. Lopez, I. Oller, M.I. Maldonado, W. Gernjak, Increased biodegradability of ultracid™ in aqueous solutions with solar TiO_2 photocatalysis, Chemosphere 68 (2007) 293–300.
[10] A. Fujishima, K. Honda, Electrochemical photolysis of water at a semiconductor electrode, Nature 238 (1972) 37–38.
[11] M.R. Bayati, F. Golestani-Fard, Photodegradation of methelyne blue over V2O5–TiO2 nanoporous layers synthesized by micro arc oxidation, Catal. Lett. 134 (2010) 162–168.

[12] R. Benedix, F.D. Jana Quaas, M. Orgass, Application of titanium dioxide photocatalysis to create self-cleaning building materials, Lacer 5 (2000) 157–168.

[13] A. Mills, S. Le Hunte, An overview of semiconductor photocatalysis, J. Photochem. Photobiol. A 108 (1997) 1–35.

[14] M. Muruganandham, N. Sobanaa, M. Swaminathan, Solar assisted photocatalytic and photochemical degradation of reactive black 5, J. Hazard. Mater. 137 (2006) 1371–1376.

[15] E. Forgacs, T. Cserháti, G. Oros, Removal of synthetic dyes from wastewaters: a review, Environ. Int. 30 (2004) 953–971.

[16] W. Liu, S. Chen, W. Zhao, S. Zhang, Study on the photocatalytic degradation of trichlorfon in suspension of titanium dioxide, Desalination 249 (2009) 1288–1293.

[17] R.L. Narayana, M. Matheswaran, A.A. Aziz, P. Saravanan, Photocatalytic decolourization of basic green dye by pure and Fe, Co doped TiO_2 under daylight illumination, Desalination 269 (2011) 249–253.

[18] C. Myung, W.J.G.H. Kim, J. Hwang, Photocatalytic properties of the transition metal doped TiO_2 powder prepared by sol–gel process, Eng. Mater. 280–283 (2007) 647–650.

[19] J. Chen, M. Yao, X.J. Wang, Investigation of transition metal ion doping behaviours on TiO_2 nanoparticles, J. Nanopart. Res. 10 (2008) 163–171.

[20] C.X. Qing, Y. Juan-yu, Z. Jun-shan, Preparation and photocatalytic properties of Fe-doped TiO_2 nanoparticles, J. Central South Univ. Technol. 11 (2004) 161–165.

[21] R. Amadelli, L. Samiolo, A. Maldotti, A. Molinari, M. Valigi, D. Gazzoli, Preparation, characterization, and photocatalytic behavior of Co–TiO_2 with visible light response, Int. J. Photoenergy 2008 (2008) 9.

[22] L. Sikong, B. Kongreong, D. Kantachote, W. Sutthisripok, Photocatalytic activity and antibacterial behavior of Fe^{3+}-doped TiO_2/SnO_2 nanoparticles, Energy Res. J. 1 (2010) 120–125.

[23] S.M. Nahar, K. Hasegawa, S. Kagaya, S. Kuroda, Comparative assessment of the efficiency of Fe-doped TiO_2 prepared by two doping methods and photocatalytic degradation of phenol in domestic water suspensions, Sci. Technol. Adv. Mater. 8 (2007) 286–291.

[24] H. Choi, M.G. Antoniou, M. Pelaez, A.A. De la Cruz, J.A. Shoemaker, D.D. Dionysiou, Mesoporous nitrogen-doped TiO_2 for the photocatalytic destruction of the cyanobacterial toxin microcystin-LR under visible light, Environ. Sci. Technol. 41 (2007) 7530–7535.

[25] Y.Q. Wang, X.J. Yu, D.Z. Sun, Synthesis, characterization and photocatalytic activity of $TiO_{2-x}N_x$ nanocatalyst, J. Hazard. Mater. 144 (2007) 328–333.

[26] M. Sathish, B. Viswanathan, R.P. Viswanath, Chinnakonda S. Gopinath, Synthesis, characterization, electronicstructure, and photocatalytic activity of nitrogen-doped TiO_2 nanocatalyst, Chem. Mater. 17 (2005) 6349–6353.

[27] S. Yin, K. Ihara, M. Komatsu, Q. Zhang, F. Saito, T. Kyotani, T. Sato, Low temperature synthesis of $TiO_{2-x}N_y$ powders and films with visible light responsive photocatalytic activity, Solid State Commun. 137 (2006) 132–137.

[28] D. Chen, Z. Jiang, J. Gen, Q. Wang, D. Yang, Carbon and nitrogen Co-doped TiO_2 with enhanced visible-light photocatalytic activity, Ind. Eng. Chem. 47 (2007) 2741–2746.

[29] R. Bacsa, J. Kiwi, T. Ohno, P. Albers, V. Nadtochenko, Preparation testing and characterization of doped TiO_2 active in the peroxidation of biomolecules under visible light, J. Phys. Chem. B 109 (2005) 5994–6003.

[30] D. Li, H. Haneda, N.K. Labhsetwar, S. Hishita, N. Ohashi, Visible-light-driven N–F–Co-doped TiO_2 photocatalysts. 1. Synthesis by spray pyrolysis and surface characterization, Chem. Phys. Lett. 401 (2005) 579–584.

[31] R. Asahi, T. Morikawa, T. Ohwaki, K. Aoki, Y. Taga, Visible-light photocatalysis in nitrogen-doped titanium oxides, Science 293 (2001) 269–271.

[32] H. Irie, Y. Watanabe, K. Hashimoto, Nitrogen-concentration dependence on photocatalytic activity of $TiO_{2-x}N_x$ powders, J. Phys. Chem. B 107 (2003) 5483–5486.

[33] M. Pelaez, A.A.D.L. Cruz, E. Stathatos, P. Falaras, D.D. Dionysiou, Visible light-activated N–F–Co-doped TiO_2 nanoparticles for the photocatalytic degradation of microcystin-LR in water, Catal. Today 144 (2009) 19–25.

[34] S. Xu, W. Shangguan, J. Yuan, M. Chen, J. Shi, Preparations and photocatalytic properties of magnetically separable nitrogen-doped TiO_2 supported on nickel ferrite, Appl. Catal. B-Environ. 71 (2007) 177–184.

[35] D. Beydoun, R. Amal, G.K.C. Low, S. McEvoy, Novel photocatalyst: titania-coated magnetite. Activity and photodissolution, J. Phys. Chem. B 104 (2000) 4387–4396.

[36] D. Beydoun, R. Amal, J. Scott, G. Low, S. McEvoy, Studies on the mineralization and separation efficiencies of a magnetic photocatalyst, Chem. Eng. Technol. 24 (2001) 745–748.

[37] D. Beydoun, R. Amal, G. Low, S. McEvoy, Occurrence and prevention of photodissolution at the phase junction of magnetite and titanium dioxide, J. Mol. Catal. A-Chem. 180 (2002) 193–200.

[38] F. Chen, Y. Xie, J. Zhao, G. Lu, Photocatalytic degradation of dyes on a magnetically separated photocatalyst under visible and UV irradiation, Chemosphere 44 (5) (2001) 1159–1168.

[39] Y. Gao, B.H. Chen, H.L. Li, Y.X. Ma, Preparation and characterization of a magnetically separated photocatalyst and its catalytic properties, Mater. Chem. Phys. 80 (2003) 348.

[40] P.W. Sellwood, Magnetochemistry, Interscience Publishers Inc., New York, 1956.

[41] J. Dharma, A. Pisal, PerkinElmer application notes UV/Vis/NIR Spectrometer, 1.

[42] E. Wang, T. He, L. Zhao, Y. Chen, Y. Gao, Improved visible light photocatalytic activity of titania doped with tin and nitrogen, J. Mater. Chem. 21 (2010) 144–150.

[43] L. Brus, Quantum crystallites and nonlinear optics, Appl. Phys. A 53 (1991) 465.

[44] M.G. Bawendi, P.J. Carrol, W.L. Wilson, Luminescence properties of cadmium selenide quantum crystallites. Resonance between interior and surface localized states, J. Chem. Phys. 96 (1992) 946–954.

[45] H.S. Wahab, T. Bredow, S.M. Aliwi, MSINDO quantum chemical modelling study of water molecule adsorption at nano-sized anatase TiO_2 surfaces, Chem. Phys. 354 (2008) 50–57.

[46] T. Sano, N. Negishi, K. Koike, K. Takeuchi, S. Matsuzawa, Preparation of a visible light-responsive photocatalyst from a complex of Ti^{4+} with a nitrogen-containing ligand, J. Mater. Chem. 14 (2004) 380–384.

[47] Y. Ao, J. Xu, S. Zhang, D. Fu, Synthesis of a magnetically separable composite photocatalyst with high photocatalytic activity under sunlight, J. Phys. Chem. Solids 70 (2009) 1042–1047.